

Photometric analysis of three totally eclipsing W UMa stars with increasing periods: TYC 3700-1384-1, V1511 Her and V1179 Her

Eric Broens¹★

¹*Vereniging Voor Sterrenkunde, Belgium*

Accepted 2020 December 19. Received 2020 December 19; in original form 2020 February 25

ABSTRACT

The first multi-colour light curve models and period studies for the totally eclipsing W UMa stars TYC 3700-1384-1, V1511 Her and V1179 Her are presented. All three stars are A-subtype W UMa stars of spectral type F. The light curve solutions show that TYC 3700-1384-1 has a moderately low mass ratio of $q = 0.182 \pm 0.001$ and a degree of overcontact of $f = 49\%$. For V1179 Her a mass ratio $q = 0.153 \pm 0.001$ and a degree of overcontact of $f = 48\%$ is derived. The solution for V1511 Her is inconclusive, however the mass ratio is expected to be between $0.13 < q < 0.15$. The evolutionary status is compared with zero-age main sequence stars taking into account energy transfer from the primary to the secondary component. The primary component of TYC 3700-1384-1 fits well in the main-sequence, while V1179 Her is more evolved. The period study reveals for all three stars a continuously increasing period at a rate of $dP/dt = 6.1 \times 10^{-7} \text{d yr}^{-1}$, $dP/dt = 5.0 \times 10^{-7} \text{d yr}^{-1}$ and $dP/dt = 9.6 \times 10^{-7} \text{d yr}^{-1}$ for TYC 3700-1384-1, V1511 Her and V1179 Her respectively. The estimated mass transfer rates derived from these period changes are $\dot{M} = 1.6 \times 10^{-7} M_{\odot} \text{yr}^{-1}$ for TYC 3700-1384-1 and $\dot{M} = 1.9 \times 10^{-7} M_{\odot} \text{yr}^{-1}$ for V1179 Her.

Key words: binaries: close – binaries: eclipsing – stars: individual (TYC 3700-1384-1, V1511 Her, V1179 Her)

1 INTRODUCTION

W UMa-type systems are contact binary stars containing two late-type dwarf stars which both fill their Roche lobes and share a common envelope. The spectral classes generally range from F to K. They are very common, among the 2.1 million variable stars that are currently included in the International Variable Star Index¹ (VSX; Watson et al. 2006), ~20% are catalogued as W UMa Stars (EW) and another ~5% are catalogued as contact binaries (EC). Most of the latter group are genuine W UMa stars too. The orbital period of W UMa stars is less than about 1 day, with typical periods of about 0.4 days. The orbital period distribution shows a sharp cut-off at 0.22 days. Few binaries, with spectral type M, have been discovered with significantly shorter periods than 0.22 days (Nefs et al. 2012; Drake et al. 2014).

Binnendijk (1970) divided W UMa stars into an A-subtype and W-subtype based on whether, respectively, the more massive component or the less massive component is eclipsed during the primary eclipse. Despite the temperatures of both stars in W UMa-type systems appear to be nearly equal, they have typically very different masses. The mass ratio can be as small as about 0.07. It proves to be challenging to develop a sound theoretical model explaining the structure of W UMa stars. Several models have been developed

but none of them provide an adequate explanation for the observed properties. Webbink (2003) gives an overview of the main structural models. The origin and evolution of W UMa stars is also still being debated. The widely held view is that they form from detached cool binaries with initial orbital periods of a few days. By a combination of evolutionary expansion and angular momentum loss arising from the magnetic stellar wind a contact binary is formed. Possibly Kozai-Lidov cycles, induced by a third body in a hierarchical triple system, shrink the orbit of an initially wider binary to orbital periods of a few days (Eggleton & Kisseleva-Eggleton 2006; Fabrycky & Tremaine 2007). Model calculations suggest that the stars in W UMa systems eventually will merge. W UMa stars are therefore considered candidate progenitors for the fast rotating FK Com Stars, Blue Stragglers and Red Novae (e.g. Bopp & Stencel 1981; Tylenda et al. 2011; Stępień & Kiraga 2015). Qian et al. (2006) and Yang & Qian (2015) suggest that W UMa stars with a low mass ratio and a high fill-out factor are particularly good candidates to evolve into rapidly rotating single stars.

Since W UMa-type binary stars are still not well understood, detailed photometric analyses and orbital period studies of those systems can provide invaluable information for further theoretical studies. A physical model that satisfactorily explains the energy and mass transfer between the two components doesn't exist yet. The presently available software models the radiative properties of the contact envelope for each component separately, based on the component's polar temperature. This causes significant discontinuities

★ E-mail: eric.broens@skynet.be

¹ <https://www.aavso.org/vsx/>

in the neck region for contact binaries with components having pronounced different temperatures. The resulting system parameters might, consequently, not be reliable in such cases (Kochoska et al. 2018). This paper presents a multi-colour light curve model and orbital period study for the totally eclipsing W UMa-type systems TYC 3700-1384-1, V1511 Her and V1179 Her. The primary and secondary eclipse depths for the stars studied in this paper are nearly equal, indicating a small temperature difference between both components, hence avoiding the problem with models caused by large discontinuities in the neck region. For totally eclipsing W UMa stars, the astrophysically important mass ratio can be obtained reliably by light curve modelling (Terrell & Wilson 2005).

2 OBSERVATIONS

Multi-colour-photometric observations have been carried out using a 20-cm Schmidt-Cassegrain telescope located in a privately owned observatory near Mol, Belgium. The telescope is equipped with a SBIG ST7-XMEI CCD camera with photometric filters. A focal reducer provides a field of view of 17 arcmin by 11 arcmin and a plate scale of $1.32 \text{ arcsec pixel}^{-1}$. The small field of view limits the number of available and suitable comparison stars of similar brightness and colour as the targets. The operating temperature of the CCD is kept constant at a temperature of about 30°C below the ambient temperature, which is between -35°C and -10°C depending on the season. The stars were kept on approximately the same pixels during an observing session by means of the CCD camera's additional auto-guider chip. Since all target stars are of similar apparent brightness, the integration time for all observations was 90s. The SNR of the comparison stars and target stars is at all times higher than 200.

The journal of observations is presented in Table 1. The initial observations have been obtained with the aim to derive the stellar parameters by modelling the light curves. The complete orbital phase is covered more than once. Later on additional observations have been acquired with the aim to obtain more times of minimum light in order to study the orbital period and to complement and verify the times of minimum light calculated from publicly available data from sky surveys. The images were processed with dark removal and flat-field corrections using the `IMRED` packages in `IRAF`². Differential photometry was performed with the `DIGIPHOT/APPHOT` package in `IRAF`. The magnitude and colours of the target and check star, transformed to the standard Johnson-Cousins system, is the average of the values obtained for each comparison star individually. The standard deviation is on average ~ 0.01 magnitude for all photometric measurements of the targets. The magnitudes and colours for the comparison stars are taken from the AAVSO Photometric All Sky Survey DR9 (APASS; Henden & Munari 2014). Since APASS does not use Cousins R_c and I_c filters, the APASS Sloan magnitudes have been transformed to $V - R_c$ and $R_c - I_c$ colours by applying the equations from Jester et al. (2005). Table 2 provides the magnitudes and colours of the used comparison and check stars for each of the observed stars. For the studied stars the measured V magnitude and $V - R_c$ and $V - I_c$ colour indices at first quadrature phase are listed. The field around TYC 3700-1384-1 was visited on 10 nights by APASS, resulting in ~ 40 measurements for each

of the comparison stars. The reported uncertainties for the selected comparison stars are $\sigma_V = 0.04$, $\sigma_{R'} = 0.1$ and $\sigma_{I'} = 0.1$. The selected comparison stars in the field of V1179 Her were measured between 26 and 40 times in total on 5 to 7 nights with uncertainties of $\sigma_V = 0.04$, $\sigma_{I'} = 0.15$ and $\sigma_{R'} = 0.04$. The field of V1511 Her was only observed on 2 nights by APASS, totalling 10 measurements for each comparison star. The listed errors are much smaller, $\sigma_V \gtrsim 0.02$, $\sigma_{I'} \approx 0.04$ and $\sigma_{R'} \approx 0.04$. The large uncertainties on the Sloan magnitudes for the fields of TYC 3700-1384-1 and V1179 Her suggest that these comparison stars are unusable for accurate photometry. Fortunately the stars discussed in this paper were among the 606 W UMa stars for which Terrell et al. (2012) measured colour indices. Their colour indices for TYC 3700-1384-1, $V - R_c = 0.46 \pm 0.01$, $V - I_c = 0.91 \pm 0.02$, and for V1179 Her, $V - R_c = 0.35 \pm 0.01$, $V - I_c = 0.69 \pm 0.01$ are in good agreement with the ones presented in this paper, $V - R_c = 0.46 \pm 0.01$, $V - I_c = 0.90 \pm 0.02$ and $V - R_c = 0.38 \pm 0.02$, $V - I_c = 0.72 \pm 0.04$ respectively. For V1511 Her however, the $V - R_c = 0.35 \pm 0.01$ and $V - I_c = 0.67 \pm 0.01$ colours reported by Terrell et al. are significantly redder, although their $B - V = 0.49 \pm 0.01$ colour index suggest a higher T_{eff} than their $V - I_c$ and $V - R_c$ indices do. The colour indices from our observations are $V - R_c = 0.27 \pm 0.02$ and $V - R_c = 0.51 \pm 0.03$. Since the field of V1511 Her was only observed on two nights by APASS, the magnitudes might be less accurate than the error estimates indicate. The APASS magnitudes appear to be accurate when they are averaged over a sufficient number of nights. The comparison stars in the field of TYC 3700-1384-1, with the exception of comparison star 1, are significantly redder than the variable. With the low galactic latitude $b \approx -6^\circ$, these comparison stars are not necessarily intrinsically red making them susceptible to variability. All comparison stars used in this study remained constant within the measurement errors during the course of the observations. As will be shown in section 3.1, the reddening for TYC 3700-1384-1 is estimated to be $E(B - V) = 0.273$. Even though the colour response of the used equipment is close to the Johnson-Cousins standard system, the significant colour differences between variable and comparison star can introduce an additional systematic error when the colour terms of the transformation are not sufficiently accurate. Table 3 provides a matrix with the averaged V magnitude and the $V - R_c$ and $V - I_c$ colour indices for the selected comparison stars in this field as measured from the other ones during one night. This table demonstrates that the transformations are accurate.

3 LIGHT CURVE ANALYSIS

The light curves were initially analysed using the Wilson-Devinney (WD) code (Wilson & Devinney 1971, 1972; Wilson 1979, 1994) implemented in the legacy version of `PHOEBE` (Prša & Zwitter 2005). The effective temperature of the more massive star, the bolometric albedos and the gravity-darkening coefficients were fixed. As will be shown in following subsections, all three stars are of spectral class F, hence the gravity-darkening coefficients have been fixed to $g_1 = g_2 = 0.32$ (Lucy 1967) and the albedos to $A_1 = A_2 = 0.5$ (Ruciński 1969) appropriate for stars with a convective envelope. The logarithmic limb-darkening law coefficients from van Hamme (1993) for a solar composition star were updated automatically during the fitting process. The modelling was performed for the VR_cI_c light curves simultaneously in mode 3, which is appropriate for overcontact systems that are not in thermal contact. The adjustable parameters were: the orbital inclination i ; the mean temperature of

² `IRAF` is distributed by the National Optical Astronomy Observatories, which are operated by the Association of Universities for Research in Astronomy, Inc., under cooperative agreement with the National Science Foundation.

Table 1. Observation log.

TYC 3700-1384-1			Number of data points			V1511 Her		Number of data points			V1179 Her		Number of data points		
date	hours	V	R_c	I_c	date	hours	V	R_c	I_c	date	hours	V	R_c	I_c	
2011 Sep 30	9.4	145	145	145	2015 Jul 09	4.9	51	51	51	2015 Jun 07	4.6	54	57	57	
2011 Oct 01	10.1	156	156	156	2015 Jul 10	2.3	26	25	26	2015 Jun 09	4.8	61	62	55	
2011 Oct 15	9.8	153	153	153	2015 Jul 11	4.6	48	42	43	2015 Jun 10	5.2	57	58	57	
2011 Oct 16	5.8	92	92	92	2015 Jul 19	5.6	60	60	60	2015 Jun 11	5.2	59	56	61	
2011 Oct 21	10.9	165	165	165	2015 Jul 25	6.2	67	66	65	2015 Jun 13	5.3	62	68	71	
2011 Oct 22	11.4	173	173	173	2015 Aug 01	6.3	68	68	68	2015 Jun 16	2.7	35	38	38	
2011 Oct 23	11.2	170	170	170	2015 Aug 05	4.3	46	45	46	2015 Jun 25	3.6	47	47	47	
2018 Jan 31	4.0	50	50	50	2015 Sep 01	6.2	65	61	60	2015 Jun 30	4.4	62	62	62	
2018 Feb 05	5.5	68	68	68	2015 Sep 20	4.5	47	47	47	2015 Jul 01	3.8	49	54	54	
2018 Feb 07	2.1	27	27	27	2017 Sep 23	4.2	55	55	55	2015 Jul 06	4.8	66	66	66	
2018 Feb 12	2.7	34	34	34	2018 Jul 23	5.8	73	73	73	2019 May 11	5.4	66	66	66	
2018 Feb 13	4.0	50	50	50	2018 Aug 01	3.7	47	47	47						
2019 Jan 20	5.8	71	71	71	2019 Aug 25	6.4	80	80	80						
					2019 Aug 26	4.9	61	61	61						
					2019 Aug 29	6.2	77	74	77						

Table 2. The coordinates, V magnitude and colours of the target stars, comparison stars and check star.

	star	α (2000.0)	δ (2000.0)	V	$V - R_c$	$V - I_c$
target	TYC 3700-1384-1	02 ^h 42 ^m 45 ^s .3	+52°59′19″.9	11.36 ± 0.01	0.46 ± 0.01	0.90 ± 0.02
comp 1	TYC 3700-0950-1	02 ^h 45 ^m 38 ^s .5	+53°02′50″.6	10.56 ± 0.04	0.22 ± 0.15	0.42 ± 0.15
comp 2	GSC 3700-1333	02 ^h 45 ^m 24 ^s .0	+53°00′27″.6	11.99 ± 0.04	0.75 ± 0.16	1.45 ± 0.16
comp 3	GSC 3700-1121	02 ^h 45 ^m 25 ^s .5	+52°57′12″.5	12.64 ± 0.04	0.94 ± 0.14	1.82 ± 0.14
check	TYC 3700-1332-1	02 ^h 45 ^m 31 ^s .9	+52°59′40″.6	11.48 ± 0.07	0.81 ± 0.07	1.56 ± 0.07
target	V1511 Her	17 ^h 55 ^m 27 ^s .4	+44°06′54″.4	11.51 ± 0.01	0.27 ± 0.02	0.51 ± 0.03
comp 1	TYC 3101-687-1	17 ^h 55 ^m 46 ^s .3	+44°08′45″.8	11.16 ± 0.01	0.26 ± 0.03	0.50 ± 0.03
comp 2	TYC 3101-1015-1	17 ^h 55 ^m 16 ^s .3	+44°01′19″.1	11.43 ± 0.02	0.40 ± 0.06	0.77 ± 0.06
comp 3	GSC 3101-1069	17 ^h 55 ^m 47 ^s .0	+44°11′02″.1	12.42 ± 0.00	0.28 ± 0.06	0.54 ± 0.06
comp 4	GSC 3101-0805	17 ^h 56 ^m 01 ^s .3	+44°02′07″.0	12.62 ± 0.01	0.28 ± 0.04	0.54 ± 0.04
check	TYC 3101-1607-1	17 ^h 55 ^m 28 ^s .2	+44°02′23″.2	13.32 ± 0.01	0.24 ± 0.08	0.48 ± 0.08
target	V1179 Her	16 ^h 27 ^m 44 ^s .9	+11°03′38″.0	11.42 ± 0.01	0.38 ± 0.02	0.72 ± 0.04
comp 1	TYC 963-108-1	16 ^h 27 ^m 45 ^s .5	+11°08′46″.3	11.14 ± 0.04	0.43 ± 0.15	0.83 ± 0.15
comp 2	TYC 963-266-1	16 ^h 28 ^m 01 ^s .7	+11°08′17″.7	12.11 ± 0.02	0.62 ± 0.16	1.20 ± 0.16
comp 3	GSC 963-96	16 ^h 27 ^m 38 ^s .1	+11°10′36″.5	12.03 ± 0.04	0.40 ± 0.16	0.78 ± 0.16
check	GSC 964-69	16 ^h 28 ^m 10 ^s .7	+11°03′32″.5	13.02 ± 0.02	0.44 ± 0.18	0.86 ± 0.16

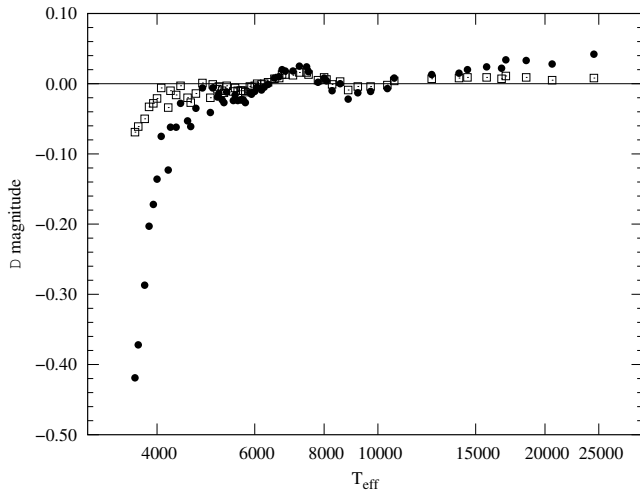
Note: For the target stars the magnitude and colours at maximum light are listed, obtained from the observations presented in this paper. The magnitude and colours for the comparison and check stars are taken from the AAVSO Photometric All Sky Survey (APASS). Refer to the text for the discussion on the low precision of the comparison stars colour indices.

star 2, T_2 ; the monochromatic luminosities of star 1, L_1 in each observed passband; and the dimensionless potential of star 1, Ω_1 ($\Omega_1 = \Omega_2$ for contact binaries, Ω will be used further in this paper). It is known that the formal errors provided by the WD code are unrealistically small. The anonymous referee pointed out that the approach of assuming a fixed temperature for one component is not adequate, and that the method outlined in Prša & Zwitter (2005) is capable to provide individual temperatures and eventually should result in the right object colour. Additionally, the error distributions should be sampled to provide reliable parameter uncertainties. Since the PHOEBE 2 versions (Prša et al. 2016; Horvat et al. 2018; Jones et al. 2020; Conroy et al. 2020) provide the feature for colour-constraining the model passband fluxes, and a Markov Chain Monte Carlo (MCMC) sampler based on EMCEE (Foreman-Mackey et al. 2013), the analysis has been re-done using PHOEBE 2. The pro-

visional values obtained with the legacy version of PHOEBE are listed in Table 4 and served as priors for the MCMC sampling. In the last row of the table the reduced χ_r^2 is provided as the sum of the reduced χ_r^2 values for the 3 passbands separately. The observed magnitudes were transformed to fluxes using a passband-independent magnitude m_0 . The value for m_0 was chosen in a way that the flux of the V light curve is of the order of unity at first quadrature phase and is given in Table 2. Next, a synthetic single A0V ($T_{\text{eff}} = 9600\text{K}$) star was created in PHOEBE 2 and the passband flux ratios f_V/f_{R_c} and f_V/f_{I_c} , based on the Castelli & Kurucz (2003) model atmospheres, were calculated to scale the observed fluxes to the Castelli & Kurucz (2003) responses in PHOEBE 2. In order to test the validity of this approach, colour indices were calculated for synthetic single stars in the range of $3550\text{K} \leq T_{\text{eff}} \leq 26000\text{K}$ and compared

Table 3. TYC 3700-1384-1 comparison star matrix.

	measured			
	comp 1	comp 2	comp 3	check
comp	V			
comp 1		11.990 ± 0.008	12.619 ± 0.018	11.470 ± 0.009
comp 2	10.554 ± 0.008		12.615 ± 0.018	11.466 ± 0.010
comp 3	10.582 ± 0.018	12.013 ± 0.018		11.494 ± 0.014
comp	$V - R_c$			
comp 1		0.759 ± 0.009	0.940 ± 0.014	0.787 ± 0.008
comp 2	0.208 ± 0.010		0.932 ± 0.015	0.779 ± 0.011
comp 3	0.218 ± 0.014	0.761 ± 0.016		0.789 ± 0.014
comp	$V - I_c$			
comp 1		1.546 ± 0.010	1.797 ± 0.014	1.524 ± 0.008
comp 2	0.414 ± 0.010		1.789 ± 0.014	1.515 ± 0.010
comp 3	0.440 ± 0.014	1.474 ± 0.015		1.542 ± 0.014

**Figure 1.** Difference of the $V - R_c$ (open squares) and $V - I_c$ (filled circles) colour indices obtained from the [Castelli & Kurucz \(2003\)](#) responses for a single dwarf star in PHOEBE 2, minus the values provided in the online table of [Pecaut & Mamajek \(2013\)](#) in function of T_{eff} .

with the colour indices given in the [Pecaut & Mamajek \(2013\)](#)³ online table, version 2019.3.22. With the exception of the extreme cooler and hotter ends of this range, the differences of the calculated colour indices are not larger than 2% as shown in Fig. 1. Since the studied stars have been observed in 3 passbands the temperatures are overdetermined. Therefore for each star two MCMC runs were executed, one for the combination of the V and R_c passband and one for the V and I_c passband.

3.1 TYC 3700-1384-1

For the initial analysis with the legacy version of PHOEBE, the effective temperature of star 1, T_1 , was estimated by fitting the spectral energy distribution (SED) to Kurucz ODFNEW/NOVER models using VOSA⁴ ([Bayo et al. 2008](#)). The best model is selected through

³ https://www.pas.rochester.edu/~emamajek/EEM_dwarf_UBVIJHK_colors_Teff.txt

⁴ <http://svo2.cab.inta-csic.es/theory/vosa/>

χ^2 minimization. Publicly available broad-band photometry from UV to IR wavelengths, as well as the photometry from the observations presented in this paper, have been used to construct the SED. To fit the SED, the surface gravity was fixed to $\log g = 4$ and the metallicity is fixed to be solar, which is justified by the study from [Rucinski et al. \(2013\)](#) showing the metallicity to be roughly solar from a sample of 52 F-type contact binaries. The SED is corrected for interstellar reddening with $E(B - V) = 0.273$ based on the reddening $E(g - r)_{PS1} = 0.279$ in the Pan-STARRS 1 passbands, provided by the Bayestar19 dustmap ([Green et al. 2019](#)) for a *Gaia* DR2 distance of $335 \pm 4 pc$ ([Gaia Collaboration et al. 2018](#)). The reddening $E(g - r)_{PS1}$ is converted to $E(B - V)$ using $E(B - V) = 0.981 E(g - r)_{PS1}$ as derived from table 6 in [Schlafly & Finkbeiner \(2011\)](#). The distance is however slightly smaller than the minimum reliable distance modulus $m - M = 8.26$ indicated for this line-of-sight. The best fit was found for a $T_{\text{eff}} = 6750 \pm 125 K$ and is plotted in Fig. 2. Fixing T_1 to this value, the photometric solution converges to a low mass ratio of $q = 0.19$, an inclination $i = 82^\circ$, a slightly cooler secondary with $T_{\text{eff}} = 6576 K$, and $\Omega = 2.15$. These values were used as priors, with reasonable uniform distributions, for the MCMC parameter space sampling. The observed fluxes were de-reddened using table 3 in [Cardelli et al. \(1989\)](#) and the effective temperature of the primary was added to the set of parameters allowed to vary freely. A corner plot of the resulting MCMC chain for the set of freely varying parameters is shown for the VR_c run in Fig. 3 and for the VI_c run in Fig. 4. The model parameters, as extracted from the posterior distributions are listed in Table 5. The last row lists the average of the obtained values with the standard deviation as uncertainty estimate. For the temperatures the largest internal errors of each component as obtained from the MCMC posterior distribution are added in quadrature. The effective temperatures for the primary and secondary component are $T_1 = 6596 \pm 98 K$ and $T_2 = 6472 \pm 106 K$ respectively. The inclination of the system $i = 80.9 \pm 0.7^\circ$ shows that the eclipses are seen nearly edge-on. The mass ratio $q = 0.182 \pm 0.001$ and $\Omega = 2.130 \pm 0.004$ reveal a moderate fill-out factor of $f = 49\%$. The light and colour curves are shown in Fig. 5. The solid line and dashed line are based on the results from the MCMC runs with the VR_c and VI_c observations respectively. The residuals of the V light curve are plotted as the flux ratio to the model from the VR_c run. Because T_{eff} is overdetermined with more than 2 bandpasses, one of the model's colour curves shows a mismatch in flux level with respect to the observations. This is as expected, unless in the unlikely case that all systematic errors are

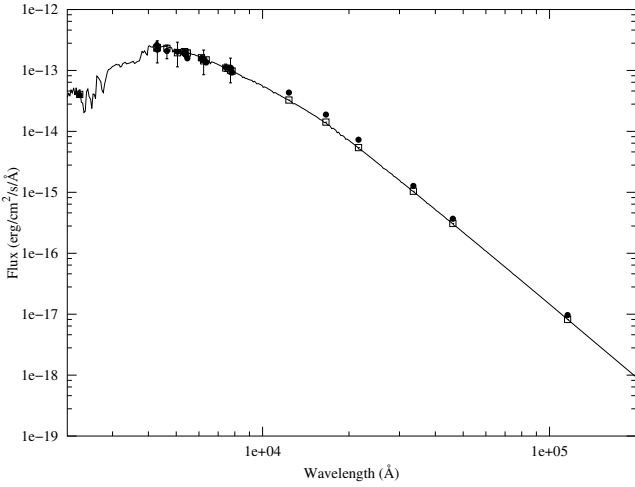


Figure 2. SED of TYC 3700-1384-1, the solid line is the Kurucz ODFNEW/NOVER model for a star with $T_{\text{eff}} = 6750\text{K}$, $\log g = 4.0$ and solar metallicity. The solid points are the fluxes calculated from the publicly available GALEX, APASS, SDSS, GAIA, 2MASS and WISE photometry, together with the VR_cI_c observations at secondary minimum presented in this paper.

negligible small. The model reproduces the shape of the observed colour curves very well.

Pasternacki et al. (2011) derived very different stellar parameters for this star based on observations with the Berlin Exoplanet Search Telescope. The results listed in their table 2 appear to be incorrect. They found a temperature difference of $\Delta T_{\text{eff}} = 670\text{K}$ between the primary and secondary star, with the primary star the cooler one. However, the light curve published in their paper cannot account for such a temperature difference because the depth of the primary and secondary eclipses are nearly equal. Also the values of the dimensionless Kopal potentials are too large.

3.2 V1511 Her

V1511 Her is included in the fourth data release (DR4⁵; Luo et al. 2018) of the Large Sky Area Multi-Object Fiber Spectroscopic Telescope (LAMOST; Cui et al. 2012; Zhao et al. 2012) regular survey. The catalogue lists an effective temperature of $T_{\text{eff}} = 6096 \pm 17\text{K}$, a $\log g = 4.2 \pm 0.03$ and a metallicity $[FE/H] = -0.04 \pm 0.01$. The $V - I_c$ colour index from our observations indicate a much higher temperature. As discussed in section 2, the APASS magnitudes for this field might not be as accurate as the uncertainties indicate because the field was only observed on two nights. Gaia DR2 lists a distance of $315 \pm 19\text{pc}$ for V1511 Her. For this distance, the Bayestar19 dust map gives a converted reddening of $E(B - V) = 0.044$. De-reddening the $V - I_c$ colour index provided by Terrell et al. (2012), $(V - I_c)_0 = 0.61$, suggest a temperature that is in good agreement with the one provided by LAMOST DR4. However, the de-reddened $(B - V)_0 = 0.45$ colour index suggest a much higher binary temperature of $\sim 6500\text{K}$, while our reddening free $(V - I_c)_0 = 0.44$ suggests a $T_{\text{eff}} \sim 6750\text{K}$. Despite these large discrepancies, a light curve analyses has been performed. Since the star exhibits total eclipses and the important mass-ratio q is not strongly correlated with the temperatures, the mass-ratio can be

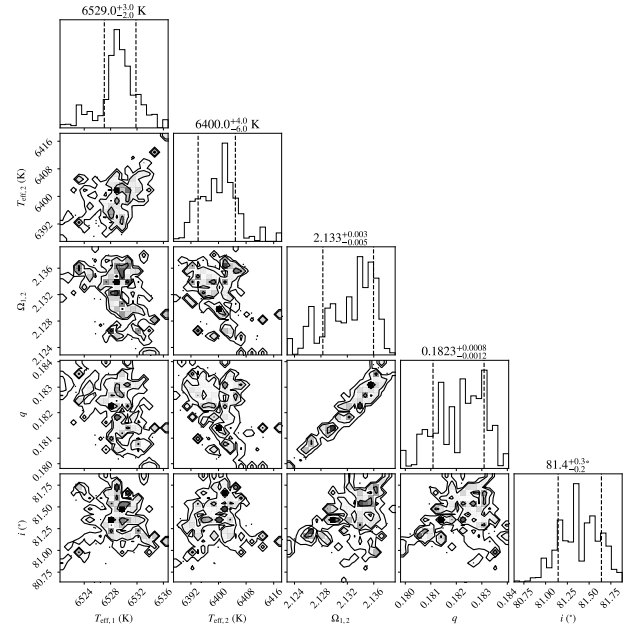


Figure 3. Corner plot depicting the PHOEBE 2 MCMC posterior distributions for the effective temperatures of the primary (T_1) and secondary (T_2), the dimensionless Kopal potential ($\Omega_{1,2}$), the mass ratio (q) and the inclination (i) from the run with the V and R_c passbands of TYC 3700-1384-1. The dashed lines indicate the 16th and 84th percentile.

derived fairly accurately. Initially the light curve has been modelled using the legacy version of PHOEBE with the temperature of the primary fixed to the value $T_{\text{eff}} = 6096\text{K}$ provided by LAMOST. The preliminary photometric solution resulted in a marginal temperature difference between the primary and the secondary, $T_2 = 6107\text{K}$, and results in a low mass ratio of $q = 0.13$ and $\Omega = 1.984$, implying a very high fill-out factor of $f = 80\%$. The inclination $i = 74^\circ.7$. A photometric solution has also been obtained in a similar way as for TYC 3700-1384-1. The parameter space was scanned using MCMC in PHOEBE 2. The values for the priors were taken from the preliminary solution obtained with the legacy version, except for the temperature of the primary. The prior for T_1 was set to 6760K in agreement with the $V - I_c$ colour index of the observations. Generous uniform distributions were used for all parameters. The corner plots of the resulting MCMC chain are shown in Fig. 6 and Fig. 7 for the VR_c and VI_c run respectively. The temperatures for the primary and secondary from this solution are $T_1 = 6793 \pm 101\text{K}$ and $T_1 = 6715 \pm 103\text{K}$. The significant difference in the colour indices with respect to those published by Terrell et al. (2012) indicate that the systematic error of the component's effective temperatures is likely much larger than the uncertainties on these temperatures indicate. The derived mass-ratio $q = 0.153 \pm 0.001$ in this solution is somewhat higher than the one obtained from the preliminary solution with the primary temperature fixed to the LAMOST DR4 binary temperature, while the inclination $i = 76^\circ.7 \pm 0^\circ.2$ is similar. The value of $\Omega = 2.063 \pm 0.004$ results in a fill-out factor $f = 49\%$ which is much smaller compared to the model with the lower temperatures. The light curve and colour curves are plotted in Fig. 8. The solid line and dashed line are based on the results from the MCMC runs with the VR_c and VI_c observations respectively. The observed colour variation is larger than calculated from the model. The amplitude of the $V - I_c$ colour variation in the preliminary

⁵ <http://cdsarc.u-strasbg.fr/viz-bin/cat/V/153>

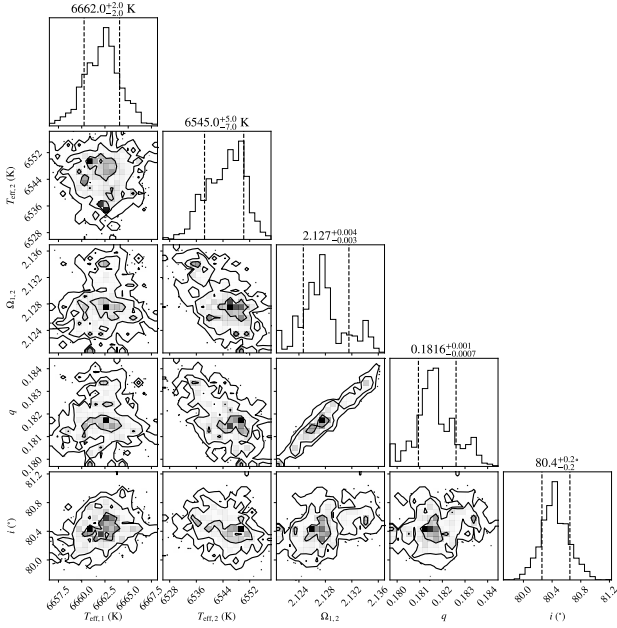


Figure 4. Same as Fig. 3 but from the run with the V and I_C passbands of TYC 3700-1384-1.

model based on the lower LAMOST DR4 temperature, is only $5mmag$ larger, and hence does not account for the observed colour variation either.

3.3 V1179 Her

LAMOST DR4 lists an effective temperature of $T_{\text{eff}} = 6249 \pm 12K$, a $\log g = 4.12 \pm 0.02$ and a metallicity $[FE/H] = -0.12 \pm 0.01$, hence the temperature of star 1 was fixed to $T_1 = 6249K$ for the initial analysis. The best photometric solution for this provisional analysis is found for $T_2 = 6085K$, a mass-ratio $q = 0.14$, $\Omega = 2.02$ and an inclination $i = 77^\circ$. These parameters were used as priors for the parameter space sampling with MCMC. The analysis was performed in the same way as for the other two studied stars. Using the reddening of $E(B - V) = 0.106$, provided by the Bayestar19 dust map for a distance of $403 \pm 5pc$ as listed by *Gaia* DR2, the observations were de-reddened by applying the passband dependent ratios given in table 3 in [Cardelli et al. \(1989\)](#). The results from the two individual MCMC runs in *PHOEBE 2* are summarized in table 5, the corner plots of the resulting MCMC chains are shown in Fig. 9 and Fig. 10. The averaged effective temperatures $T_1 = 6171 \pm 135K$ and $T_2 = 6034 \pm 117K$ for the primary and secondary respectively, are consistent with the binary temperature provided by LAMOST DR4. The binary has a low mass-ratio $q = 0.153 \pm 0.001$, $\Omega = 2.067 \pm 0.04$, an inclination $i = 77^\circ.2 \pm 0^\circ.6$ and a moderate fill-out factor of $f = 45\%$. The light curve and the residuals are shown in Fig. 11. The models colour curves are in good agreement with the observed ones. The residuals are plotted as the flux ratio of the V observations to the model flux calculated with the results of the VI_C run.

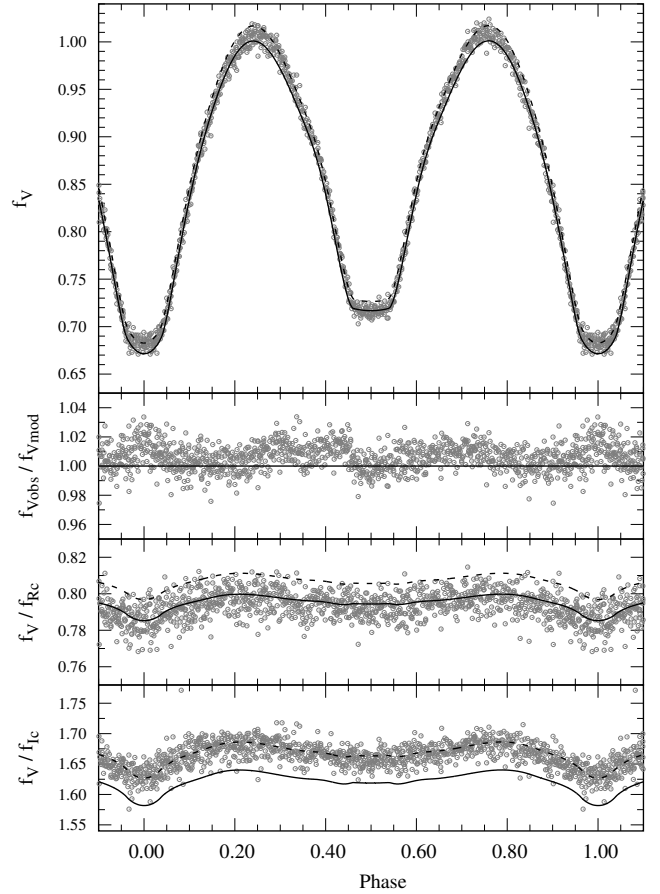


Figure 5. V light curve of TYC 3700-1384-1 as normalized flux. The solid line is the synthetic light curve based on the results of the MCMC run with the VR_C observations and the dashed line on the run with the VI_C observations. The lower panels display the residuals as the flux ratio of the V observations to the VR_C model, and the colour curves respectively.

4 ECLIPSE TIMINGS AND ORBITAL PERIOD STUDY

Times of minimum light are calculated for the observations presented in this paper, and for publicly available observations from Super Wide Angle Search for Planets (SWASP; [Butters et al. 2010](#)), Northern Sky Variability Survey (NSVS; [Woźniak et al. 2004](#)), All-Sky Automated Survey All Star Catalogue (ASAS-3; [Pojmanski 2002](#)) and All Sky Automated Survey for SuperNovae (ASAS-SN; [Shappee et al. 2014](#)), if available for the studied star. For V1179 Her also times of minima from [Diethelm \(2007, 2008, 2010\)](#) and [Hubscher \(2016\)](#) are included.

Many studies use the Kwee-van Woerden method (KVV; [Kwee & van Woerden 1956](#)) to calculate the times of minimum light. The KVV method assumes symmetric minima which is not always the case for binaries exhibiting star spot activity. Moreover, it is well known that this method underestimates the uncertainties. In order to get more accurate uncertainty estimates, the times of minimum light are calculated with following procedure. For the observations presented in this paper, and the time series observations from SWASP, first the times of minimum light are estimated by eye from the light curves. Next, the observations limited to a time interval of $\pm 0.25P$ around the estimated time of minimum light, are fitted to the obtained model light curves with *PHOEBE* by shifting them in time, and also in magnitude for the SWASP observations. By limiting

Table 4. Light curve solutions from the provisional analysis.

	TYC 3700-1384-1	V1511 Her	V1179 Her
$g_1 = g_2$	0.32	0.32	0.32
$A_1 = A_2$	0.5	0.5	0.5
$x_{1bol} = x_{2bol}$	0.657	0.650	0.649
$y_{1bol} = y_{2bol}$	0.189	0.139	0.156
$x_{1V} = x_{2V}$	0.698	0.729	0.728
$y_{1V} = y_{2V}$	0.287	0.274	0.273
$x_{1R} = x_{2R}$	0.605	0.636	0.636
$y_{1R} = y_{2R}$	0.287	0.278	0.278
$x_{1I} = x_{2I}$	0.514	0.545	0.544
$y_{1I} = y_{2I}$	0.270	0.263	0.263
T_1	6750 K	6096 K	6249 K
T_2	6576 K	6107 K	6085 K
$q = m_2/m_1$	0.192	0.132	0.143
i	82.07	74.66	77.05
Ω	2.152	1.984	2.023
Ω_i	2.214	2.054	2.084
Ω_o	2.091	1.968	1.991
f	50%	80%	66%
χ_r^2	3.01	2.34	6.18

Table 5. Best fit models from the MCMC sampling.

Run	T_1	T_2	q	i	Ω	Ω_i	Ω_o	f
TYC 3700-1384-1								
VR_c	$6529^{+3}_{-2}K$	$6400^{+4}_{-6}K$	$0.1823^{+0.0008}_{-0.0012}$	$81^\circ 4^{+0.3}_{-0.2}$	$2.133^{+0.003}_{-0.005}$	2.188	2.071	47%
VI_c	$6662^{+2}_{-2}K$	$6545^{+3}_{-3}K$	$0.1816^{+0.001}_{-0.0007}$	$80^\circ 4^{+0.2}_{-0.2}$	$2.127^{+0.004}_{-0.003}$	2.186	2.070	50%
average	$6596 \pm 98K$	$6472 \pm 106K$	0.182 ± 0.001	$80^\circ 9 \pm 0.7$	2.130 ± 0.004	2.187	2.071	49%
V1511 Her								
VR_c	$6730^{+10}_{-10}K$	$6650^{+20}_{-20}K$	$0.155^{+0.002}_{-0.002}$	$76^\circ 8^{+0.4}_{-0.4}$	$2.067^{+0.003}_{-0.005}$	2.117	2.017	49%
VI_c	$6856^{+6}_{-6}K$	$6780^{+10}_{-20}K$	$0.154^{+0.002}_{-0.002}$	$76^\circ 9^{+0.4}_{-0.5}$	$2.065^{+0.008}_{-0.009}$	2.114	2.015	49%
average	$6793 \pm 101K$	$6715 \pm 103K$	0.154 ± 0.001	$76^\circ 8 \pm 0.1$	2.066 ± 0.001	2.114	2.014	48%
V1179 Her								
VR_c	$6080^{+4}_{-5}K$	$5956^{+4}_{-8}K$	$0.152^{+0.002}_{-0.002}$	$77^\circ 6^{+0.2}_{-0.1}$	$2.064^{+0.004}_{-0.007}$	2.108	2.010	45%
VI_c	$6263^{+3}_{-3}K$	$6113^{+8}_{-8}K$	$0.154^{+0.002}_{-0.002}$	$76^\circ 7^{+0.2}_{-0.2}$	$2.070^{+0.007}_{-0.004}$	2.113	2.014	44%
average	$6171 \pm 135K$	$6034 \pm 117K$	0.153 ± 0.001	$77^\circ 2 \pm 0.6$	2.067 ± 0.004	2.111	2.012	45%

the observations to a time interval of $\pm 0.25P$ around the estimated minimum, the times for individual primary and secondary minima can be calculated separately. The timings from the observations presented in this paper are weighted averages of the minima calculated from the V , R_c and I_c light curves independently. NSVS, ASAS-3 and ASAS-SN only provide a few observations nightly. Therefore the observations for a complete observation season have been phased before fitting them to the model light curves.

The uncertainty of the obtained time of minimum light is estimated by the weighted median difference in time between the observations and the model light curve. The weights are assigned based on the local slope of the model curve, assigning small or even zero weight to the observations around minimum and maximum light and allow for a reliable uncertainty estimate on the time of minimum light. In order to demonstrate this, the reduced χ_r^2 values are calculated from a linear regression fit to the times of minima for V1511 Her, obtained for the three seasons of SWASP data separately. The re-

duced χ_r^2 statistic for the 76 times of minima in the timespan of $2453141 < HJD < 2453272$, the 16 times of minima in the timespan $2454297 < HJD < 2454336$ and the 60 times of minima in the time period of $2454586 < HJD < 2454688$ are $\chi_r^2 = 1.65$, $\chi_r^2 = 2.17$ and $\chi_r^2 = 0.74$ respectively.

4.1 TYC 3700-1384-1

Gettel et al. (2006) derived a period of $0^d.40745944$ from the NSVS observations but no detailed period study is published so far. Table 7 lists the times of minimum light calculated from NSVS, ASAS-SN, SWASP and the observations presented in this paper. From these timings the following least-squares ephemeris is obtained:

$$HJD \text{ Min } I = 2455835.4930(9) + 0^d.4074723(2) \times E \quad (1)$$

The $O - C$ residuals calculated with these ephemeris are plotted in Fig. 12. The $O - C$ diagram indicates a linearly increasing period. A

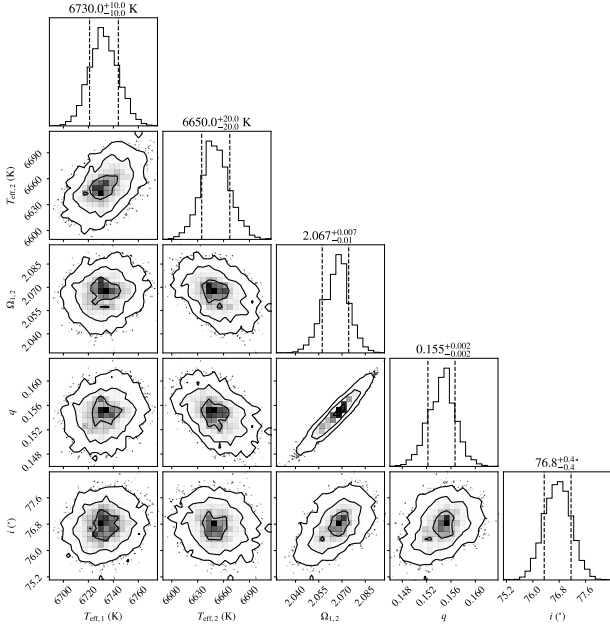


Figure 6. Corner plot depicting the PHOEBE 2 MCMC posterior distributions for the effective temperatures of the primary (T_1) and secondary (T_2), the dimensionless Kopal potential ($\Omega_{1,2}$), the mass ratio (q) and the inclination (i) from the run with the V and R_C passbands of V1511 Her. The dashed lines indicate the 16th and 84th percentile.

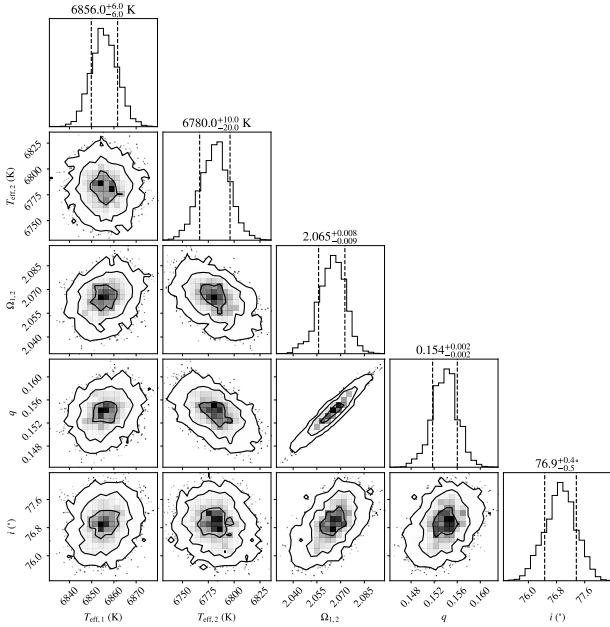


Figure 7. Same as Fig. 6 for the V and I_C passbands of V1511 Her.

quadratic least-square fit to the minima light times yields following ephemeris:

$$HJD \text{ Min } I = 2455835.4868(3) + 0^d 40747202(5) \times E + 3.7(1) \times 10^{-10} \times E^2 \quad (2)$$

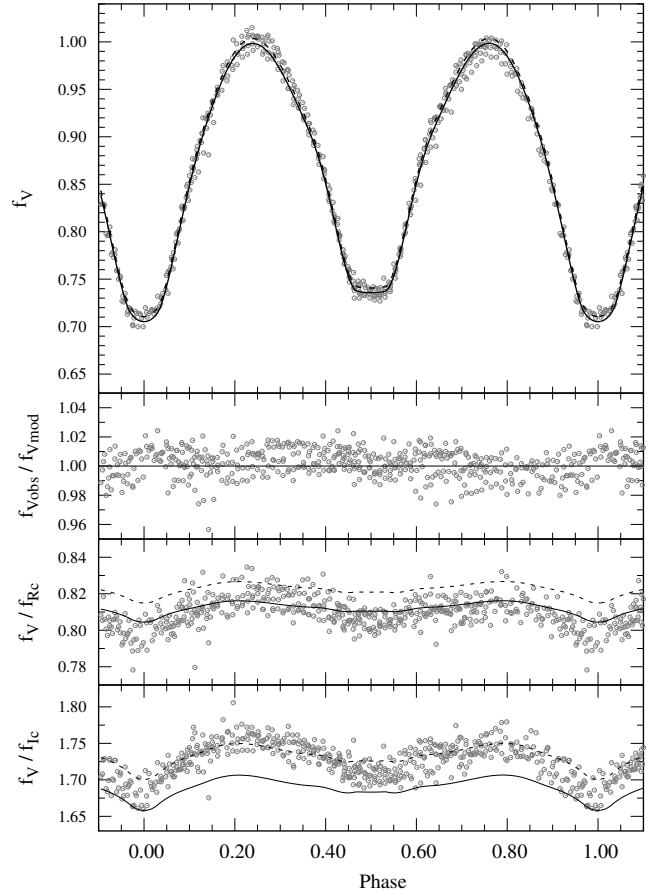


Figure 8. V light curve of V1511 Her as normalized flux. The solid line is the synthetical light curve based on the results of the MCMC run with the $V R_C$ observations and the dashed line on the run with the $V I_C$ observations. The lower panels display the residuals as the flux ratio of the V observations to the $V R_C$ model, and the colour curves respectively.

From the quadratic term, a continuous period increase rate of $dP/dt = 6.1 \times 10^{-7} d \text{ yr}^{-1}$, or $0.05 s \text{ yr}^{-1}$ is derived.

4.2 V1511 Her

V1511 Her was discovered as a contact binary by [Akerlof et al. \(2000\)](#) and they published a period of $0^d 35005 \pm 0^d 00004$ based on ROTSE-I observations between March 15th and June 15th 1999. [Gettel et al. \(2006\)](#) published a period of $0^d 3500768$ based on the complete dataset of ROTSE-I observations spanning about 1 year. Observations of this star are publicly available from NSVS, ASAS-SN and SWASP. The times of minimum light obtained from these observations and our observations are listed in Table 6. From all these timings we derived the following linear ephemeris:

$$HJD \text{ Min } I = 2457223.4091(9) + 0^d 3500769(1) \times E \quad (3)$$

The $O - C$ values based on this ephemeris plotted in Fig. 13 suggests a continuously increasing period. A quadratic fit to these times of minima yields following ephemeris:

$$HJD \text{ Min } I = 2457223.4084(2) + 0^d 35007946(5) \times E + 2.54(4) \times 10^{-10} \times E^2 \quad (4)$$

implying a continuous period increase rate of $dP/dt = 5.0 \times 10^{-7} d \text{ yr}^{-1}$ or $0.04 s \text{ yr}^{-1}$. No observations nor times of min-

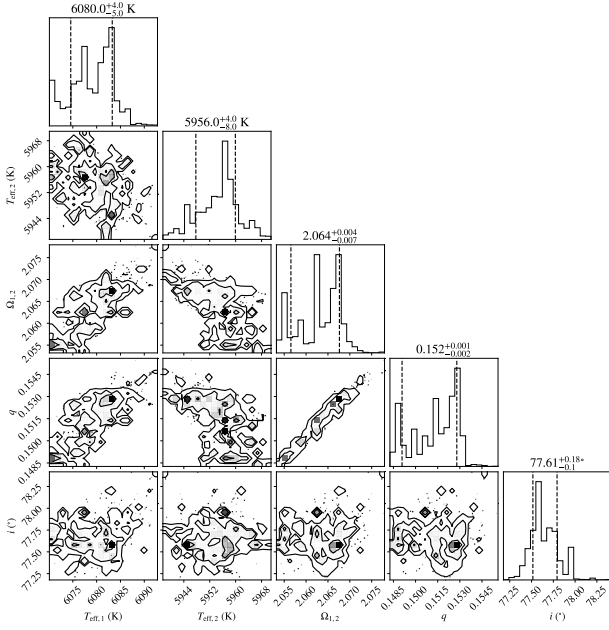


Figure 9. Corner plot depicting the PHOEBE 2 MCMC posterior distributions for the effective temperatures of the primary (T_1) and secondary (T_2), the dimensionless Kopal potential ($\Omega_{1,2}$), the mass ratio (q) and the inclination (i) from the run with the V and R_C passbands of V1179 Her. The dashed lines indicate the 16th and 84th percentile.

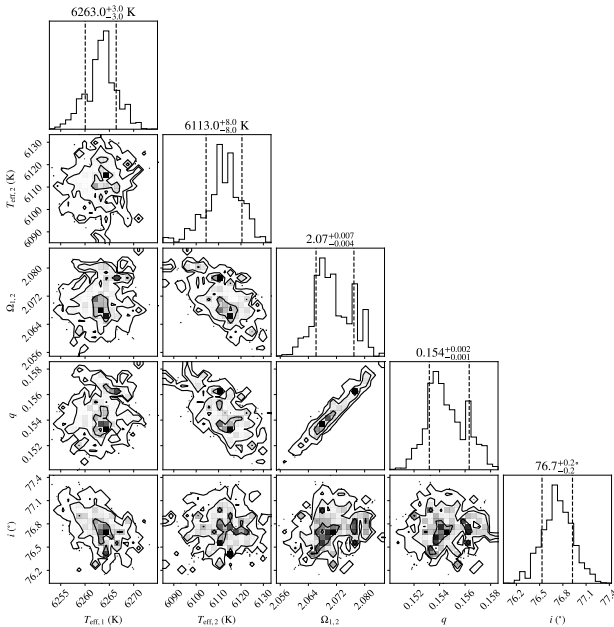


Figure 10. Same as Fig. 9 for the V and I_C passbands of V1179 Her.

ima light are available for the period between 2000 and 2004, and between 2009 and 2013. We cannot exclude that instead of a continuously increasing period, there are multiple sudden period changes. The times of minima between 2004 and 2009 and between 2013 and the present can be equally well fitted with respectively follow-

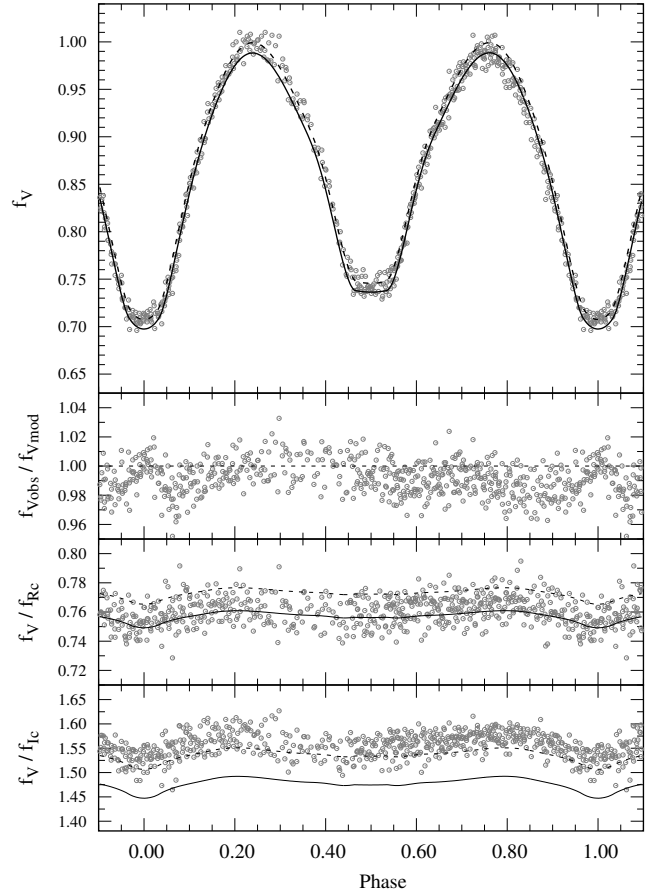


Figure 11. V light curve of V1179 Her as normalized flux. The solid line is the synthetical light curve based on the results of the MCMC run with the $V R_C$ observations and the dashed line on the run with the $V I_C$ observations. The lower panels display the residuals as the flux ratio of the V observations to the $V I_C$ model, and the colour curves respectively.

ing linear ephemeris: $-11660 \leq E \leq -7240$:

$$HJD \text{ Min } I = 2457223.3867(4) + 0^{\text{d}}.35007465(5) \times E \quad (5)$$

$-2150 \leq E \leq 4300$:

$$HJD \text{ Min } I = 2457223.4081(3) + 0^{\text{d}}.3500806(1) \times E \quad (6)$$

4.3 V1179 Her

V1179 Her has also been discovered by [Akerlof et al. \(2000\)](#) and they published a period of $0^{\text{d}}.38545 \pm 0^{\text{d}}.00003$. Since this star is at a declination of $+11^\circ$, the star has also been observed by the ASAS-3 from the Las Campanas Observatory in Chile. [Pojmanski \(2002\)](#) published a period of $0^{\text{d}}.385493$ based on the ASAS-3 observations. The observations collected by NSVS, ASAS-3, ASAS-SN are publicly available. Unlike the two other stars studied in this paper, no observations are available from SWASP. The calculated times of minimum light are listed in Table 8 together with those published by [Diethelm \(2007, 2008, 2010\)](#) and [Hubscher \(2016\)](#). Following linear ephemeris are derived from these observations:

$$HJD \text{ Min } I = 2457184.408(3) + 0^{\text{d}}.3855008(4) \times E \quad (7)$$

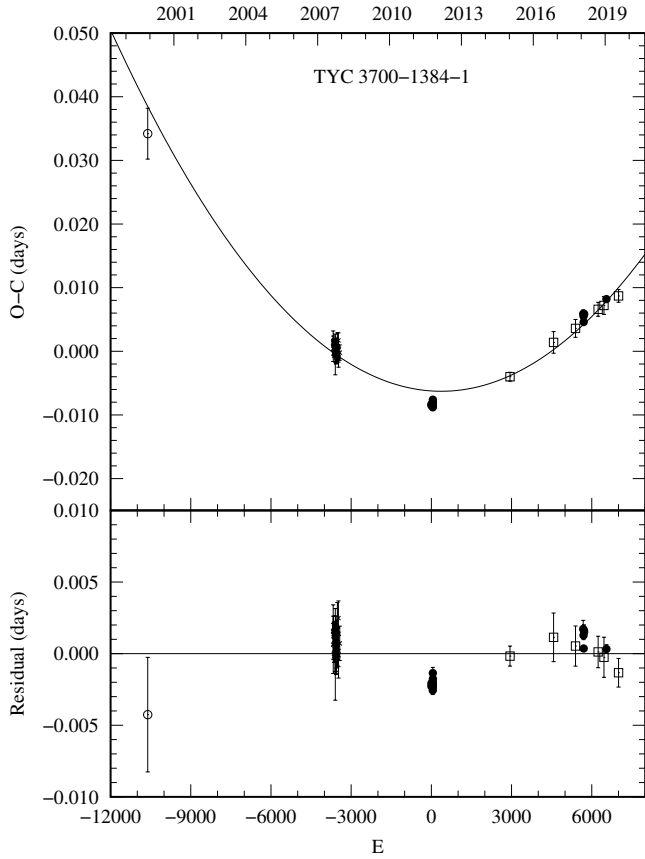


Figure 12. $O - C$ diagram of TYC 3700-1384-1. Open circles, NSVS data; crosses, SWASP data; open squares ASAS-SN data; filled circles, this paper.

The $O - C$ diagram plotted in Fig. 14 clearly shows the signature of a linearly increasing period. The quadratic ephemeris is:

$$HJD \text{ Min } I = 2457184.4058(4) + 0^d 3855056(1) \times E + 5.2(1) \times 10^{-10} \times E^2 \quad (8)$$

implying a continuous period increase of $dP/dt = 9.6 \times 10^{-7} \text{ d yr}^{-1}$, or 0.08 s yr^{-1} .

5 RESULTS AND CONCLUSION

Photometric observations were obtained in the V , R_c and I_c passbands for the three W UMa stars TYC 3700-1384-1, V1511 Her and V1179 Her. Since the orbital planes of the observed W UMa stars are aligned closely enough to our line-of-sight to manifest total eclipses, and the primary and secondary eclipse depths are similar indicating a small temperature difference between both components, stellar parameters can be determined reliably from the photometric observations. Comparison star magnitudes from APASS DR9 were used. The Sloan r' and i' magnitudes given in APASS are transformed to the Johnson-Cousins $V - R_c$ and $R_c - I_c$ colours using the equations from Jester et al. (2005). The uncertainties, $\sigma_{r'} = 0.1$ and $\sigma_{i'} = 0.1$, for the comparison stars in the fields of TYC 3700-1384-1 and $\sigma_{r'} = 0.15$ in the field of V1179 Her are large. Despite these large uncertainties, the colour indices for TYC 3700-1384-1 and V1179 Her presented in this paper are in excellent agreement with the ones obtained by Terrell et al. (2012) using all-sky photometry. The uncertainties for the comparison stars in the field of V1511

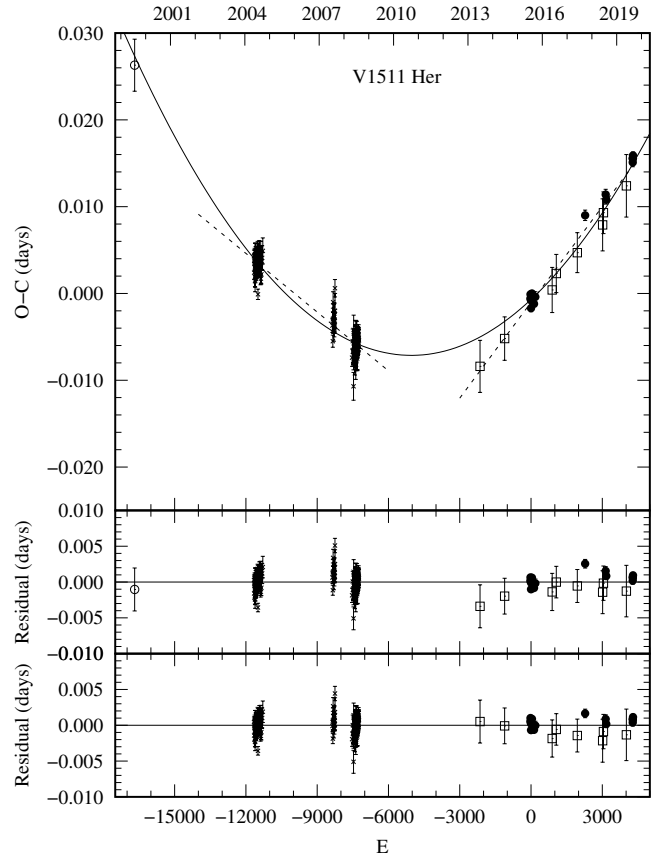


Figure 13. $O - C$ diagram of V1511 Her. The dashed lines refer to the linear ephemeris given in equations 5 and 6. Middle panel, residuals of the $O - C$ values with respect to the quadratic ephemeris; lower panel, residuals with respect to the linear ephemerides. Symbols are the same as in Fig. 12.

Her, $\sigma_V \gtrsim 0.02$, $\sigma_{r'} \approx 0.04$ and $\sigma_{i'} \approx 0.04$ are much smaller, but the field has only been observed on 2 nights resulting in 10 measurements for each star. In contrast to these small uncertainties, the resulting $V - R_c$ and $V - I_c$ colour indices for V1511 Her are inconsistent with those from Terrell et al. (2012).

The light curves in the three passbands were initially modelled simultaneously using the WD method implemented in the legacy version of PHOEBE. These resulting provisional system parameters were subsequently used in PHOEBE 2 for further analysis. The model passband fluxes were colour constrained in order to derive temperatures for both components individually, without a priori assumptions, from the photometric observations transformed to the Johnson-Cousins standard system. The photometric observations were converted to fluxes using a passband independent magnitude m_0 , and next in PHOEBE 2 scaled according to the Castelli & Kurucz (2003) passband responses. Although PHOEBE 2.2 supports interstellar reddening and extinction (Jones et al. 2020), the photometric measurements were de-reddened using table 3 in Cardelli et al. (1989). The uncertainties on the derived system parameters are estimated in PHOEBE 2 using the Markov Chain Monte Carlo (MCMC) method implemented via emcee. Since the observations have been made in 3 passbands, the temperatures are overdetermined. Therefore for each star two MCMC runs were executed, one with the VR_c observations and one with the VI_c observations. The results are summarised in Table 5. The derived temperatures show that all three systems are of F-type spectral class. The temperature

Table 6. Times of minima of V1511 Her.

Epoch	HJD	data*	Epoch	HJD	data*	Epoch	HJD	data*
-16682.0	2451383.4526 ± 0.0030	(1)	-11434.5	2453220.4599 ± 0.0010	(4)	-7364.0	2454645.4358 ± 0.0010	(4)
-11659.5	2453141.6918 ± 0.0007	(4)	-11426.0	2453223.4339 ± 0.0009	(4)	-7363.5	2454645.6124 ± 0.0011	(4)
-11654.0	2453143.6153 ± 0.0008	(4)	-11423.0	2453224.4850 ± 0.0006	(4)	-7361.0	2454646.4851 ± 0.0010	(4)
-11634.0	2453150.6179 ± 0.0009	(4)	-11417.5	2453226.4091 ± 0.0011	(4)	-7358.0	2454647.5361 ± 0.0012	(4)
-11631.0	2453151.6684 ± 0.0009	(4)	-11414.5	2453227.4606 ± 0.0006	(4)	-7352.0	2454649.6382 ± 0.0012	(4)
-11628.5	2453152.5443 ± 0.0008	(4)	-11411.5	2453228.5111 ± 0.0008	(4)	-7349.5	2454650.5147 ± 0.0010	(4)
-11625.5	2453153.5937 ± 0.0011	(4)	-11406.0	2453230.4364 ± 0.0006	(4)	-7346.5	2454651.5633 ± 0.0010	(4)
-11622.5	2453154.6447 ± 0.0006	(4)	-11403.0	2453231.4861 ± 0.0008	(4)	-7344.0	2454652.4377 ± 0.0010	(4)
-11617.0	2453156.5677 ± 0.0011	(4)	-11386.0	2453237.4376 ± 0.0005	(4)	-7335.0	2454655.5881 ± 0.0010	(4)
-11614.0	2453157.6174 ± 0.0012	(4)	-11383.0	2453238.4858 ± 0.0011	(4)	-7332.5	2454656.4660 ± 0.0010	(4)

*data: (1) NSVS (Woźniak et al. 2004), (3) ASAS-SN (Shappee et al. 2014), (4) SWASP (Butters et al. 2010), (5) this paper.

For minima observed in more than one passband the weighted mean of the timings in those passbands is listed.

A machine-readable version of this table is online available in its entirety with this publication. A portion is shown here for guidance regarding its form and content.

Table 7. Times of minima of TYC 3700-1384-1.

Epoch	HJD	data*	Epoch	HJD	data*	Epoch	HJD	data*
-10610.0	2451512.2461 ± 0.0040	(1)	-3551.0	2454388.5581 ± 0.0010	(4)	53.5	2455857.2846 ± 0.0004	(5)
-3676.0	2454337.6262 ± 0.0005	(4)	-3548.5	2454389.5782 ± 0.0010	(4)	54.0	2455857.4882 ± 0.0003	(5)
-3673.5	2454338.6448 ± 0.0019	(4)	-3541.0	2454392.6328 ± 0.0008	(4)	54.5	2455857.6926 ± 0.0004	(5)
-3671.0	2454339.6626 ± 0.0020	(4)	-3538.5	2454393.6524 ± 0.0008	(4)	56.0	2455858.3028 ± 0.0003	(5)
-3651.5	2454347.6090 ± 0.0008	(4)	-3516.5	2454402.6174 ± 0.0022	(4)	56.5	2455858.5072 ± 0.0004	(5)
-3649.0	2454348.6270 ± 0.0006	(4)	-3509.5	2454405.4690 ± 0.0007	(4)	2942.0	2457034.2725 ± 0.0007	(3)
-3646.5	2454349.6463 ± 0.0007	(4)	-3507.0	2454406.4873 ± 0.0008	(4)	4572.0	2457698.4578 ± 0.0017	(3)
-3644.0	2454350.6636 ± 0.0006	(4)	-3504.5	2454407.5064 ± 0.0010	(4)	5393.0	2458032.9947 ± 0.0014	(3)
-3641.5	2454351.6837 ± 0.0008	(4)	-3477.5	2454418.5098 ± 0.0012	(4)	5681.5	2458150.5528 ± 0.0006	(5)
-3624.5	2454358.6102 ± 0.0012	(4)	-3475.0	2454419.5262 ± 0.0011	(4)	5693.5	2458155.4420 ± 0.0003	(5)
-3619.5	2454360.6477 ± 0.0009	(4)	-3472.5	2454420.5445 ± 0.0016	(4)	5698.0	2458157.2748 ± 0.0002	(5)
-3617.0	2454361.6659 ± 0.0006	(4)	-3428.5	2454438.4740 ± 0.0012	(4)	5710.5	2458162.3695 ± 0.0004	(5)
-3614.5	2454362.6849 ± 0.0009	(4)	0.0	2455835.4845 ± 0.0004	(5)	5713.0	2458163.3880 ± 0.0003	(5)
-3600.0	2454368.5924 ± 0.0014	(4)	2.5	2455836.5034 ± 0.0004	(5)	6238.0	2458377.3118 ± 0.0011	(3)
-3592.5	2454371.6483 ± 0.0032	(4)	36.5	2455850.3573 ± 0.0004	(5)	6457.0	2458466.5488 ± 0.0014	(3)
-3568.0	2454381.6308 ± 0.0009	(4)	37.0	2455850.5611 ± 0.0004	(5)	6550.0	2458504.4448 ± 0.0003	(5)
-3565.5	2454382.6519 ± 0.0007	(4)	39.0	2455851.3761 ± 0.0003	(5)	7004.0	2458689.4377 ± 0.0010	(3)
-3563.0	2454383.6683 ± 0.0011	(4)	51.5	2455856.4693 ± 0.0004	(5)			
-3553.5	2454387.5409 ± 0.0008	(4)	52.0	2455856.6728 ± 0.0003	(5)			

*data: (1) NSVS (Woźniak et al. 2004), (2) ASAS-3 (Pojmanski 2002), (3) ASAS-SN (Shappee et al. 2014), (5) this paper.

For minima observed in more than one passband the weighted mean of the timings in those passbands is listed.

differences between the components for all three stars are small as one can expect from the nearly equal primary and secondary eclipse depths. This makes the obtained system parameters less prone to the model discontinuities in the contact region of the binary (Kochoska et al. 2018). For all three systems the more massive component is eclipsed during the primary eclipse, hence the stars are of A-subtype according to the Binnendijk (1970) classification.

For TYC 3700-1381-1 the derived effective temperatures for the primary and secondary are $T_1 = 6596 \pm 98K$ and $T_2 = 6472 \pm 106K$ respectively. The temperatures and are in good agreement with the effective binary temperature $T_{\text{eff}} = 6500 \pm 125K$ estimated from the SED using a wide range of wavelengths. The uncertainties on these temperatures are consistent with the uncertainties on the observed colour indices. The small mass-ratio $q = 0.182 \pm 0.001$ and dimensionless potential $\Omega = 2.130 \pm 0.004$ indicate a moderate fill-out factor of $f = 49\%$. The derived orbital inclination $i = 80.9 \pm 0.7^\circ$. The uncertainties are estimated from the standard deviation of the

values provided by the two MCMC runs in PHOEBE 2. The resulting model light and colour curves from the best solution of both runs are plotted in Fig. 5. Because T_{eff} is overdetermined with more than 2 bandpasses, one of the model's colour curves shows a mismatch in flux level with respect to the observations. This is as expected, unless in the unlikely case that all systematic errors are negligible small. As can be seen in Fig. 5 the observed colour variations are well reproduced by the model.

As shown in Fig. 11, the model light and colour curves for V1179 Her are also in good agreement with the observations. The averaged system parameters from the two MCMC runs are: $T_1 = 6171 \pm 135K$, $T_2 = 6034 \pm 117K$, $q = 0.153 \pm 0.001$, $\Omega = 2.067 \pm 0.04$ and $i = 77.2 \pm 0.6^\circ$. The fill-out factor $f = 45\%$. The temperatures are consistent with the $T_{\text{eff}} = 6249 \pm 12K$ given in LAMOST DR4 for the binary. The PHOEBE 2 MCMC posterior distributions for the run with the VR_c and VI_c light curves are plotted in Fig. 9 and Fig. 10 respectively.

Table 8. Times of minima of V1179 Her.

Epoch	HJD	data*	Epoch	HJD	data*	Epoch	HJD	data*
-15152.0	2451343.3432 ± 0.0042	(1)	-8503.0	2453906.4903 ± 0.0007	(6)	-2.5	2457183.4415 ± 0.0006	(5)
-14453.0	2451612.8029 ± 0.0016	(1)	-8492.5	2453910.5352 ± 0.0007	(6)	0.0	2457184.4046 ± 0.0004	(5)
-11435.0	2452776.2167 ± 0.0036	(2)	-7540.0	2454277.7241 ± 0.0039	(2)	3.0	2457185.5618 ± 0.0004	(5)
-10492.0	2453139.7371 ± 0.0044	(2)	-7494.0	2454295.4543 ± 0.0005	(7)	8.0	2457187.4898 ± 0.0003	(5)
-9503.0	2453520.9928 ± 0.0045	(2)	-7434.5	2454318.3951 ± 0.0002	(7)	39.0	2457199.4408 ± 0.0004	(5)
-8627.5	2453858.4941 ± 0.0003	(6)	-6613.0	2454635.0820 ± 0.0067	(2)	52.0	2457204.4522 ± 0.0004	(5)
-8622.0	2453860.6138 ± 0.0061	(2)	-5680.0	2454994.7542 ± 0.0079	(2)	67.5	2457210.4273 ± 0.0004	(5)
-8578.5	2453877.3860 ± 0.0040	(6)	-5473.5	2455074.3618 ± 0.0006	(8)	884.0	2457525.1928 ± 0.0019	(3)
-8534.0	2453894.5374 ± 0.0008	(6)	-1866.0	2456465.0537 ± 0.0010	(3)	1842.0	2457894.5085 ± 0.0020	(3)
-8529.0	2453896.4629 ± 0.0013	(6)	-909.0	2456833.9816 ± 0.0016	(3)	2794.0	2458261.5127 ± 0.0018	(3)
-8524.0	2453898.3971 ± 0.0011	(6)	-59.0	2457161.6604 ± 0.0016	(3)	2799.0	2458263.4402 ± 0.0025	(3)
-8523.5	2453898.5831 ± 0.0016	(6)	-15.5	2457178.4275 ± 0.0020	(9)	3712.0	2458615.4114 ± 0.0004	(5)
-8518.5	2453900.5100 ± 0.0006	(6)	-7.5	2457181.5136 ± 0.0005	(5)	3761.0	2458634.3007 ± 0.0021	(3)

*data: (1) NSVS (Woźniak et al. 2004), (2) ASAS-3 (Pojmanski 2002), (3) ASAS-SN (Shappee et al. 2014), (4) SWASP (Butters et al. 2010), (5) this paper, (6) (Diethelm 2007), (7) (Diethelm 2008), (8) (Diethelm 2010), (9) (Hubscher 2016).

For minima observed in more than one passband the weighted mean of the timings in those passbands is listed.

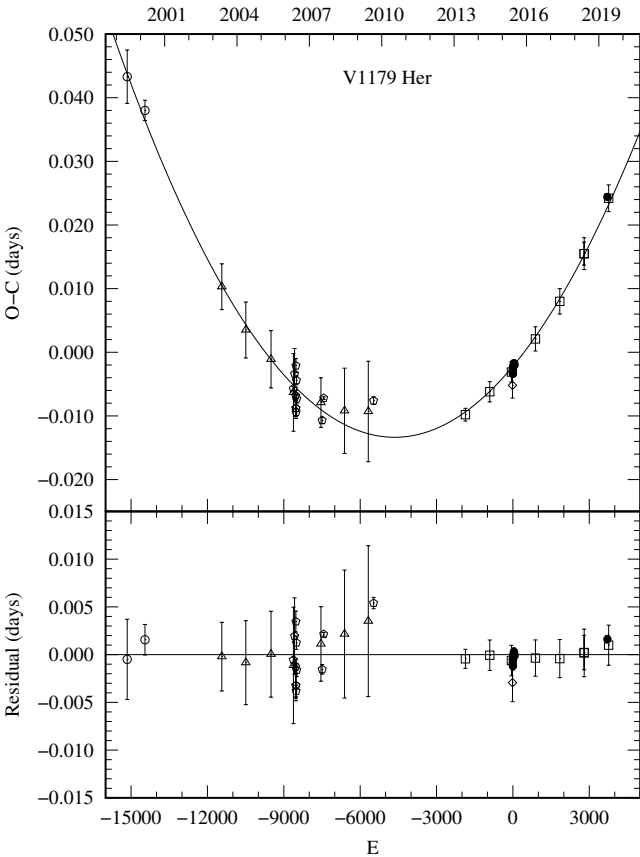


Figure 14. $O - C$ diagram of V1179 Her. Symbols are the same as in Fig. 12, with additionally open triangles, ASAS-3 data; open pentagons, (Diethelm 2007, 2008, 2010); open diamonds, (Hubscher 2016).

While the uncertainties of the APASS comparison stars in the field of V1511 Her are reasonable, our measured colour indices are inconsistent with the ones provided by Terrell et al. (2012). The reddening free $(V - Ic)_0 = 0.61$ from the observations of Terrell et al. (2012) suggest a temperature that is in good agree-

ment with $T_{\text{eff}} = 6096 \pm 17K$ provided by LAMOST DR4. However, the reddening free $(B - V)_0 = 0.45$ colour index from Terrell et al. (2012) suggest a much higher binary temperature of $T_{\text{eff}} \sim 6500K$. From the MCMC run in PHOEBE 2, effective temperatures $T_1 = 6793 \pm 101K$ and $T_2 = 6715 \pm 103K$ are derived, which are significantly higher than the binary temperature given by LAMOST DR4. The uncertainties provided here are consistent with the errors on the derived colour indices, but don't account for a possibly larger systematic error in the values of the comparison stars provided in APASS DR9. The derived mass-ratio $q = 0.154 \pm 0.001$ and the value of $\Omega = 2.066 \pm 0.001$, resulting in a fill-out factor $f = 48\%$, is somewhat higher than the mass-ratio $q = 0.13$ from the preliminary solution with the primary temperature fixed to the temperature given by LAMOST DR4. The inclination $i = 76^\circ 8' \pm 0^\circ 1'$. The amplitude of the model colour curve based on the results from the MCMC runs, plotted in Fig. 8, does not match the observed colour changes. Also the model fitted with the legacy version of PHOEBE, with T_1 fixed to the value $T_{\text{eff}} = 6096K$ provided by LAMOST DR4, does not reproduce the amplitude of the colour changes completely. The amplitude for the $V - Ic$ colour curve is only $5mmag$ larger. From this initial analysis a temperature of $T_2 = 6107K$ is obtained for secondary, and the very low mass ratio $q = 0.13$ and $\Omega = 1.984$ imply a very high fill-out factor of $f = 80\%$. With the derived temperatures, and the model colour curves, being inconsistent, the results for this system are inconclusive.

The period study based on the times of minimum light presented in this paper, and calculated from the publicly available observations and those available in the literature show that all three stars have a linearly increasing period. The period of TYC 3700-1384-1 is increasing by $dP/dt = 6.1 \times 10^{-7} d yr^{-1}$ which equals 5 seconds per century, the period of V1511 Her by $dP/dt = 5.0 \times 10^{-7} d yr^{-1}$ or 4 seconds per century and the period of V1179 Her by $dP/dt = 9.6 \times 10^{-7} d yr^{-1}$ or 8 seconds per century. Due to the lack of minimum timings between 2000 and 2004 and between 2009 and 2013 it cannot be excluded that the period change of V1511 Her is composed of multiple discrete period changes. Linearly increasing periods are usually attributed to mass transfer from the less massive component to the more massive one through the neck of the system.

Using the distance provided by Gaia DR2 and taking the reddening

obtained from the Bayestar19 3D dust map into account, the luminosities for the primary components in these systems are calculated. The bolometric corrections are taken from the [Pecaut & Mamajek \(2013\)](#) online table, version 2019.3.22. The nearly equal effective temperatures of both components in W UMa stars despite their very different masses, is often explained by energy transfer from the more massive to the less massive star. [Mochnicki \(1981\)](#) defined a quantity U as the transferred component of the secondary's luminosity expressed as the fraction of the energy radiated from the surface of the primary. This quantity allows to correct the luminosity, and the temperature of the primary at constant radius, for the energy transfer in order to compare the primaries with zero-age main sequence stars. Fig. 15 depicts the positions of the primaries in the HR diagram, and their positions when corrected for the energy transfer to other A and W-subtype primaries taken from [Yakut & Eggleton \(2005\)](#). The filled squares indicate the positions with the observed properties and the filled circles the positions corrected for energy transfer. The primary component of TYC 3700-1384-1 fits well in the main sequence, while the primary of V1179 Her appears to be more evolved. Despite the analysis of V1511 Her is inconclusive, the primary is plotted, with smaller symbols, in Fig. 15. The uncertainty on the *Gaia* distance for this star is also ~ 5 times larger than for the other two studied stars, while the distances are similar. The position in the HR diagram based on the provisional solution with T_1 fixed to the temperature from LAMOST DR4 is indicated with $2r$ in the plot, while the bluer solution derived from the observed colour indices is indicated with $2b$. The bluer solution falls well below the ZAMS, hence favoring the provisional solution based on the cooler temperature from LAMOST DR4. The primary temperatures corrected for energy transfer, $T_1^c = 6888K$ and $T_1^c = 6405K$ for TYC 3700-1384-1 and V1179 Her respectively, suggest a primary mass of $M_1 = 1.45M_\odot$ for TYC 3700-1384-1 and $M_1 = 1.3M_\odot$ for V1179 Her. The mass transfer rates from the less massive component to the more massive one are estimated using these masses and the derived period change rates. For TYC 3700-1384-1 the mass transfer rates amounts to $\dot{M} = 1.6 \times 10^{-7} M_\odot yr^{-1}$ and for V1179 Her to $\dot{M} = 1.9 \times 10^{-7} M_\odot yr^{-1}$.

ACKNOWLEDGEMENTS

The author would like to thank the anonymous referee for giving valuable suggestions and comments that resulted in a significant improvement of the manuscript. Special thanks are due to Dr. Kyle Conroy for the support provided on using PHOEBE 2 to model the studied stars. This research made use of the International Variable Star Index (VSX) data base, operated at AAVSO, Cambridge, Massachusetts, USA. Additionally this study made use of NASA's Astrophysics Data System, and the SIMBAD and VizieR data bases operated at the CDS, Strasbourg, France.

DATA AVAILABILITY

The observations presented in this paper are available upon request from the author. Part of this paper makes use of publicly available data collected by SuperWide Angle Search for Planets (<https://wasp.cerit-sc.cz/form>), Northern Sky Variability Survey (<https://skydot.lanl.gov/nsvs/nsvs.php>), All-Sky Automated Survey All Star Catalogue (<http://www.astrouw.edu.pl/asas/?page=asas3>) and All Sky Automated Survey for SuperNovae (<https://asas-sn.osu.edu/>).

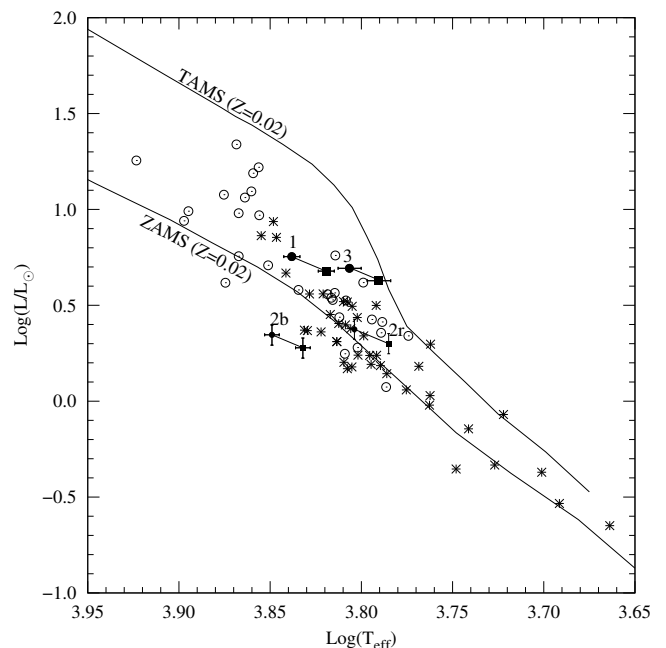


Figure 15. Positions of A-subtype (open circles) and W-subtype (asterisks) primaries, corrected for energy transfer, in the HR diagram. The positions of the stars discussed in this paper (1, TYC 3700-1384-1; 2r & 2b, V1511 Her; 3, V1179 Her) are plotted with filled circles and connected to filled squares which depict the positions without the correction for energy transfer. The solid lines are the ZAMS and TAMS from [Girardi et al. \(2000\)](#).

REFERENCES

- Akerlof C., et al., 2000, *AJ*, **119**, 1901
 Bayo A., Rodrigo C., Barrado Y Navascués D., Solano E., Gutiérrez R., Morales-Calderón M., Allard F., 2008, *A&A*, **492**, 277
 Binnendijk L., 1970, *Vistas in Astronomy*, **12**, 217
 Bopp B. W., Stencel R. E., 1981, *ApJ*, **247**, L131
 Butters O. W., et al., 2010, *A&A*, **520**, L10
 Cardelli J. A., Clayton G. C., Mathis J. S., 1989, *ApJ*, **345**, 245
 Castelli F., Kurucz R. L., 2003, in Piskunov N., Weiss W. W., Gray D. F., eds, Vol. 210, *Modelling of Stellar Atmospheres*. p. A20 ([arXiv:astro-ph/0405087](https://arxiv.org/abs/astro-ph/0405087))
 Conroy K. E., et al., 2020, *ApJS*, **250**, 34
 Cui X.-Q., et al., 2012, *Research in Astronomy and Astrophysics*, **12**, 1197
 Diethelm R., 2007, *Information Bulletin on Variable Stars*, **5781**, 1
 Diethelm R., 2008, *Information Bulletin on Variable Stars*, **5837**, 1
 Diethelm R., 2010, *Information Bulletin on Variable Stars*, **5920**, 1
 Drake A. J., et al., 2014, *ApJ*, **790**, 157
 Eggleton P. P., Kisseleva-Eggleton L., 2006, *Ap&SS*, **304**, 75
 Fabrycky D., Tremaine S., 2007, *ApJ*, **669**, 1298
 Foreman-Mackey D., Hogg D. W., Lang D., Goodman J., 2013, *PASP*, **125**, 306
 Gaia Collaboration et al., 2018, *A&A*, **616**, A1
 Gettel S. J., Geske M. T., McKay T. A., 2006, *AJ*, **131**, 621
 Girardi L., Bressan A., Bertelli G., Chiosi C., 2000, *A&AS*, **141**, 371
 Green G. M., Schlafly E., Zucker C., Speagle J. S., Finkbeiner D., 2019, *ApJ*, **887**, 93
 Henden A., Munari U., 2014, *Contributions of the Astronomical Observatory Skalnaté Pleso*, **43**, 518
 Horvat M., Conroy K. E., Pablo H., Hambleton K. M., Kochoska A., Giannararo J., Prša A., 2018, *ApJS*, **237**, 26
 Hubscher J., 2016, *Information Bulletin on Variable Stars*, **6157**, 1
 Jester S., et al., 2005, *AJ*, **130**, 873
 Jones D., et al., 2020, *ApJS*, **247**, 63
 Kochoska A., Prša A., Zwitter T., Horvat M., Conroy K. E., 2018, *arXiv*

- e-prints, p. [arXiv:1804.08781](https://arxiv.org/abs/1804.08781)
- Kwee K. K., van Woerden H., 1956, *Bull. Astron. Inst. Netherlands*, **12**, 327
- Lucy L. B., 1967, *Z. Astrophys.*, **65**, 89
- Luo A. L., Zhao Y. H., Zhao G., et al. 2018, *VizieR Online Data Catalog*, p. [V/153](#)
- Mochnecki S. W., 1981, *ApJ*, **245**, 650
- Nefs S. V., et al., 2012, *MNRAS*, **425**, 950
- Pasternacki T., et al., 2011, *AJ*, **142**, 114
- Pecaut M. J., Mamajek E. E., 2013, *ApJS*, **208**, 9
- Pojmanski G., 2002, *Acta Astron.*, **52**, 397
- Prša A., Zwitter T., 2005, *ApJ*, **628**, 426
- Prša A., et al., 2016, *ApJS*, **227**, 29
- Qian S., Yang Y., Zhu L., He J., Yuan J., 2006, *Ap&SS*, **304**, 25
- Ruciński S. M., 1969, *Acta Astron.*, **19**, 245
- Rucinski S. M., Pribulla T., Budaj J., 2013, *AJ*, **146**, 70
- Schlafly E. F., Finkbeiner D. P., 2011, *ApJ*, **737**, 103
- Shappee B., et al., 2014, in *American Astronomical Society Meeting Abstracts #223*. p. 236.03
- Stępień K., Kiraga M., 2015, *A&A*, **577**, A117
- Terrell D., Wilson R. E., 2005, *Ap&SS*, **296**, 221
- Terrell D., Gross J., Cooney W. R., 2012, *AJ*, **143**, 99
- Tylenda R., et al., 2011, *A&A*, **528**, A114
- Watson C. L., Henden A. A., Price A., 2006, *Society for Astronomical Sciences Annual Symposium*, **25**, 47
- Webbink R. F., 2003, in *Turcotte S., Keller S. C., Cavallo R. M., eds, Astronomical Society of the Pacific Conference Series Vol. 293, 3D Stellar Evolution*. p. 76 ([arXiv:astro-ph/0304420](https://arxiv.org/abs/astro-ph/0304420))
- Wilson R. E., 1979, *ApJ*, **234**, 1054
- Wilson R. E., 1994, *PASP*, **106**, 921
- Wilson R. E., Devinney E. J., 1971, *ApJ*, **166**, 605
- Wilson R. E., Devinney E. J., 1972, *ApJ*, **171**, 413
- Woźniak P. R., et al., 2004, *AJ*, **127**, 2436
- Yakut K., Eggleton P. P., 2005, *ApJ*, **629**, 1055
- Yang Y.-G., Qian S.-B., 2015, *AJ*, **150**, 69
- Zhao G., Zhao Y.-H., Chu Y.-Q., Jing Y.-P., Deng L.-C., 2012, *Research in Astronomy and Astrophysics*, **12**, 723
- van Hamme W., 1993, *AJ*, **106**, 2096